nature communications



Article

https://doi.org/10.1038/s41467-025-58726-1

Long-term physical exercise facilitates putative glymphatic and meningeal lymphatic vessel flow in humans

Received: 19 July 2024

Accepted: 26 March 2025

Published online: 09 April 2025

Check for updates

Roh-Eul Yoo 1,2,12 , Jun-Hee Kim 0,12 , Hyo Youl Moon 4,12 , Jae Yeon Park 0,4 , Seongmin Cheon 5,6 , Hyun-Suk Shin 6 , Dohyun Han 6,7,8 , Yukyoum Kim 6,7,8 , Sung-Hong Park $^{0,13} \boxtimes$ & Seung Hong Choi $^{0,12,10,11,13} \boxtimes$

Regular voluntary exercise has been shown to increase waste transport through the glymphatic system in mice. Here, we investigate the impact of physical exercise on both upstream and downstream brain waste clearance in healthy volunteers via noninvasive MR imaging. Putative glymphatic influx, evaluated using intravenous contrast-enhanced dynamic T1 mapping, increases significantly at the putamen after 12 weeks of long-term exercise using a cycle ergometer. The putative meningeal lymphatic vessel size and flow, measured by intravenous contrast-enhanced black-blood imaging and IR-ALADDIN technique, increase significantly after long-term exercise. Plasma proteomics reveals significant changes in inflammation-related and immunerelated proteins (down-regulated: S100A8, S100A9, PSMA3, and DEFA1A3; upregulated: I chain) after long-term exercise, which correlate with putative glymphatic influx or mLV flow. Our results suggest that increased glymphatic and mLV flow may be the potential mechanism underlying the neuroprotective effects of exercise on cognition, highlighting the importance of long-term, regular exercise.

The field of brain waste clearance has undergone significant advancements over the past decade, particularly with the discovery and characterization of the glymphatic system and meningeal lymphatic vessels (mLVs)¹⁻³. In the glymphatic system, a glia-dependent system of perivascular channels plays a pivotal role in eliminating toxic proteins in the interstitial fluid (ISF) by transporting them to the cerebrospinal fluid (CSF)⁴. Discharged waste products in the CSF can be cleared through the mLVs, a key downstream drainage route for CSF, into the deep cervical

lymph nodes^{5,6}. These brain clearance systems play crucial roles in maintaining central nervous system (CNS) homeostasis by facilitating the removal of toxic waste products from the brain. Recent studies have shown that the impaired brain clearance systems could be related to the accumulation of toxic proteins in the brain, such as amyloid-beta, alphasynuclein, and phosphorylated tau⁷⁻¹¹. Consequently, the impaired brain clearance systems are rapidly emerging as important pathophysiology related to neurodegenerative disease progression^{12,13}.

¹Department of Radiology, Seoul National University College of Medicine, Seoul, South Korea. ²Department of Radiology, Seoul National University Hospital, Seoul, South Korea. ³Medical Research Center, Seoul National University, Seoul, South Korea. ⁴Department of Physical Education, Seoul National University, Seoul, South Korea. ⁵School of Biological Sciences and Technology, Chonnam National University, Gwangju, Republic of Korea. ⁶Proteomics Core Facility, Biomedical Research Institute, Seoul National University Hospital, Seoul, Republic of Korea. ⁷Department of Transdisciplinary Medicine, Seoul National University Hospital, Seoul, Republic of Korea. ⁸Department of Medicine, Seoul University College of Medicine, Seoul, Republic of Korea. ⁹Department of Bio and Brain Engineering, Korea Advanced Institute of Science and Technology (KAIST), Daejeon, South Korea. ¹⁰Center for Nanoparticle Research, Institute for Basic Science (IBS), Seoul, Republic of Korea. ¹¹School of Chemical and Biological Engineering, Seoul National University, Seoul, Republic of Korea. ¹²These authors contributed equally: Roh-Eul Yoo, Jun-Hee Kim, Hyo Youl Moon. ¹³These authors jointly supervised this work: Yukyoum Kim, Sung-Hong Park, Seung Hong Choi. ¹²e-mail: ykim22@snu.ac.kr; sunghongpark@kaist.ac.kr; verocay1@snu.ac.kr

Table 1 | Baseline characteristics of the participants

Characteristics	Single- bout (<i>n</i> = 21)	Long- term (<i>n</i> = 16)	P value ^c
Age (y) ^a	24 (22–38)	27 (25–30)	0.90
Sex			1.00
Male	13	10	
Female	8	6	
Height (cm) ^b	172.9 ± 8.4	170.0 ± 8.6	0.50
Weight (kg) ^a	70.0 (62.2-72.3)	61.8 (53.0–80.3)	0.31
VO _{2max} (ml/kg/min) ^b	46.9 ± 8.9	43.1 ± 6.5	0.16

Data are reported as medians (IQRs).

The clearance of toxic and catabolic waste byproducts cannot be completed independently by the glymphatic system or mLVs^{12,13}. This highlights the need for a comprehensive understanding of the clearance system, including the structural and functional characterization of both the glymphatic system and mLVs.

Intravenous contrast-enhanced dynamic T1 mapping has shown potential in the quantitative evaluation of putative glymphatic activity in the brain¹⁴. Intravenous contrast-enhanced black-blood (BB) imaging has also demonstrated reliable applications in structural mapping of the mLVs in the brain¹⁵⁻¹⁸. In addition, inversion-recovery alternate ascending (Asc)/descending (Dsc) directional navigation technique (IR-ALADDIN), an arterial spin labeling technique, was previously shown to be effective in generating structural images and measuring the flow velocity of the putative mLVs adjacent to the superior sagittal sinus (SSS)¹⁹.

Recent studies have shown that lifestyle habits, such as physical exercise or good quality sleep, can enhance the function of the brain clearance system¹⁴. Regular voluntary exercise has been shown to enhance waste transport through the glymphatic system in mice by promoting the expression and polarization of astrocytic aquaporin-4 water channels^{20,21}. These studies support the hypothesis that regular exercise enhances the brain clearance system, which in turn may help delay the progression of cognitive impairment in individuals with neurodegenerative diseases.

Despite the accumulating knowledge, the effect of physical exercise on brain waste clearance in humans remains to be fully elucidated. In this study, we aimed to quantitatively evaluate the effects of physical exercise on putative glymphatic and mLV flow, by employing dynamic T1 mapping, BB imaging, and IR-ALADDIN in healthy normal volunteers. Investigating the effects of short-term and long-term exercise protocols on glymphatic and mLV flow via noninvasive MR imaging techniques could provide valuable insights into preventing and treating various neurodegenerative diseases.

Results

Participant characteristics

Of the 47 eligible participants, 10 participants were excluded due to failure to complete the scheduled exercise sessions (n=8), mild side effects of a gadolinium-based contrast agent (GBCA) (n=1), and dental artifacts (n=1). As a result, the single-bout exercise group included 21 participants (median age, 24 years [IQR, 22–38 years]; 13 male, 8 female) and the long-term exercise group included 16 participants (median age, 27 years [IQR, 25–30 years]; 10 male, 6 female) (Supplementary Fig. 1). There was no evidence of differences in age (P=0.90), sex (P=1.00), height (P=0.50), weight (P=0.31) or VO_{2max} (P=0.16) between the single-bout and long-term exercise groups (Table 1). Details of the results of the IPAQ (International Physical Activity Questionnaire) questionnaire are provided in the supplementary information.

Comparison of blood pressure, heart rate, putative glymphatic and mLV flow between pre- and post-exercise states

There were no significant changes in systolic and diastolic blood pressures (BPs), mean arterial pressure, or heart rate (HR) between the pre- and post-exercise states in either group (Supplementary Table 2).

 $\Delta T I_{influx}$ at the putamen increased from 25.7 ms (IQR, 24.3–34.2 ms) to 34.7 ms (IQR, 31.4–40.7 ms) after exercise in the long-term exercise group ($P\!=\!0.01$) (Fig. 1 and Table 2). However, in the single-bout exercise group, $\Delta T I_{influx}$ at the putamen did not significantly differ between the pre-exercise (30.3 ms [IQR, 25.4–39.6 ms]) and post-exercise states (28.4 ms [IQR, 19.4–41.4 ms]) ($P\!=\!0.72$) (Fig. 1 and Table 2). $\Delta T I_{efflux}$ at the putamen did not significantly differ between the pre-exercise and post-exercise states in either the single-bout ($P\!=\!0.74$) or long-term ($P\!=\!0.64$) exercise groups (Fig. 1 and Table 2). In addition, there was no evidence of differences in $\Delta T I_{influx}$ and $\Delta T I_{efflux}$ values at the cerebral cortex between the pre-exercise and post-exercise states in either the single-bout or long-term exercise groups (all $P\!>\!0.05$) (Table 2).

BB imaging could not be obtained for two participants in the single-bout group and for four participants in the long-term group due to scan failures. The putative mLV region of interest (ROI) size measured using BB imaging significantly increased after exercise in the long-term exercise group (pre-exercise: 15.0 mm^2 [IQR, $12.0-18.5 \text{ mm}^2$]; post-exercise: 21.5 mm^2 [IQR, $19.0-26.9 \text{ mm}^2$]) (P=0.008) but not in the single-bout exercise group (pre-exercise: 17.5 mm^2 [IQR, $12.0-24.0 \text{ mm}^2$]; post-exercise: 20.0 mm^2 [IQR, $16.0-24.0 \text{ mm}^2$]) (P=0.63) (Figs. 2 and 3). An intraclass correlation coefficient of the putative mLV ROI size in BB imaging was 0.87 (95% confidence interval: 0.46-0.96). A similar trend was observed for the putative mLV ROI size measured using IR-ALADDIN imaging (Figs. 2 and 4).

An increase in average percent signal change (PSC) was observed after exercise in the long-term exercise group (pre-exercise: 4.3% [IQR, 3.2-5.0%]; post-exercise: 6.1% [IQR, 4.3-7.0%]) (P=0.008) (Fig. 4). However, no difference was found in the single-bout exercise group between the pre- and post-exercise states (pre-exercise: 4.1% [IQR, 3.4-5.2%]; post-exercise: 4.7% [IQR, 3.4-5.7%]) (P=0.49) (Fig. 4).

The putative mLV flow, calculated from mLV ROI size and PSC, did not significantly differ between the pre- and post-exercise states in the single-bout exercise group (pre-exercise: $37.4 \,\mathrm{mm}^3/\mathrm{s}$ [IQR, $23.4-48.3 \,\mathrm{mm}^3/\mathrm{s}$]; post-exercise: $44.0 \,\mathrm{mm}^3/\mathrm{s}$ [IQR, $31.0-52.0 \,\mathrm{mm}^3/\mathrm{s}$]) (P=0.09) (Fig. 4). However, in the long-term exercise group, a significant increase in putative mLV flow was observed after exercise (pre-exercise: $31.4 \,\mathrm{mm}^3/\mathrm{s}$ [IQR, $22.3-42.4 \,\mathrm{mm}^3/\mathrm{s}$]; post-exercise: $36.6 \,\mathrm{mm}^3/\mathrm{s}$ [IQR, $29.2-47.9 \,\mathrm{mm}^3/\mathrm{s}$]) (P=0.002) (Fig. 4).

Correlation between differentially expressed proteins and MR imaging metrics of putative glymphatic and mLV Flow

Blood plasma samples were collected from a total of 37 individuals, both before and after exercise, resulting in 74 samples. The protein extracted from the plasma was submitted filter aided sample preparation (FASP) digestion. The peptide samples were re-dissolved in 10 µL of solvent A (0.1 formic acid in MS-grade water) and spiked with the indexed Retention Time (iRT) kit (Biognosys AG). For the data-independent acquisition (DIA) analysis, 1µg of each sample was analyzed using a Q-Exactive Plus (Thermo Fisher Scientific) equipped with an Ultimate 3000 UHPLC system. The DIA file was processed in Spectronaut using the default setting. After spectrum processing, a total of 672 proteins were quantified from the samples, excluding the spike-in internal retention time (iRT) standards used for calibration. By using an adjusted P value (false discovery rate) less than 0.05 to define differentially expressed proteins (DEPs) before and after exercises, 26 DEPs were identified in the single-bout exercise group, while 17 DEPs were identified in the long-term exercise group. Among these DEPs from the longterm exercise group, two proteins were significantly changed after exercise in both the single-bout exercise group and the long-term

bData are means + SDs.

^cThe P values were calculated using the two-sided Fisher exact test for categorical variables and the two-sided Mann-Whitney U-test for continuous variables.

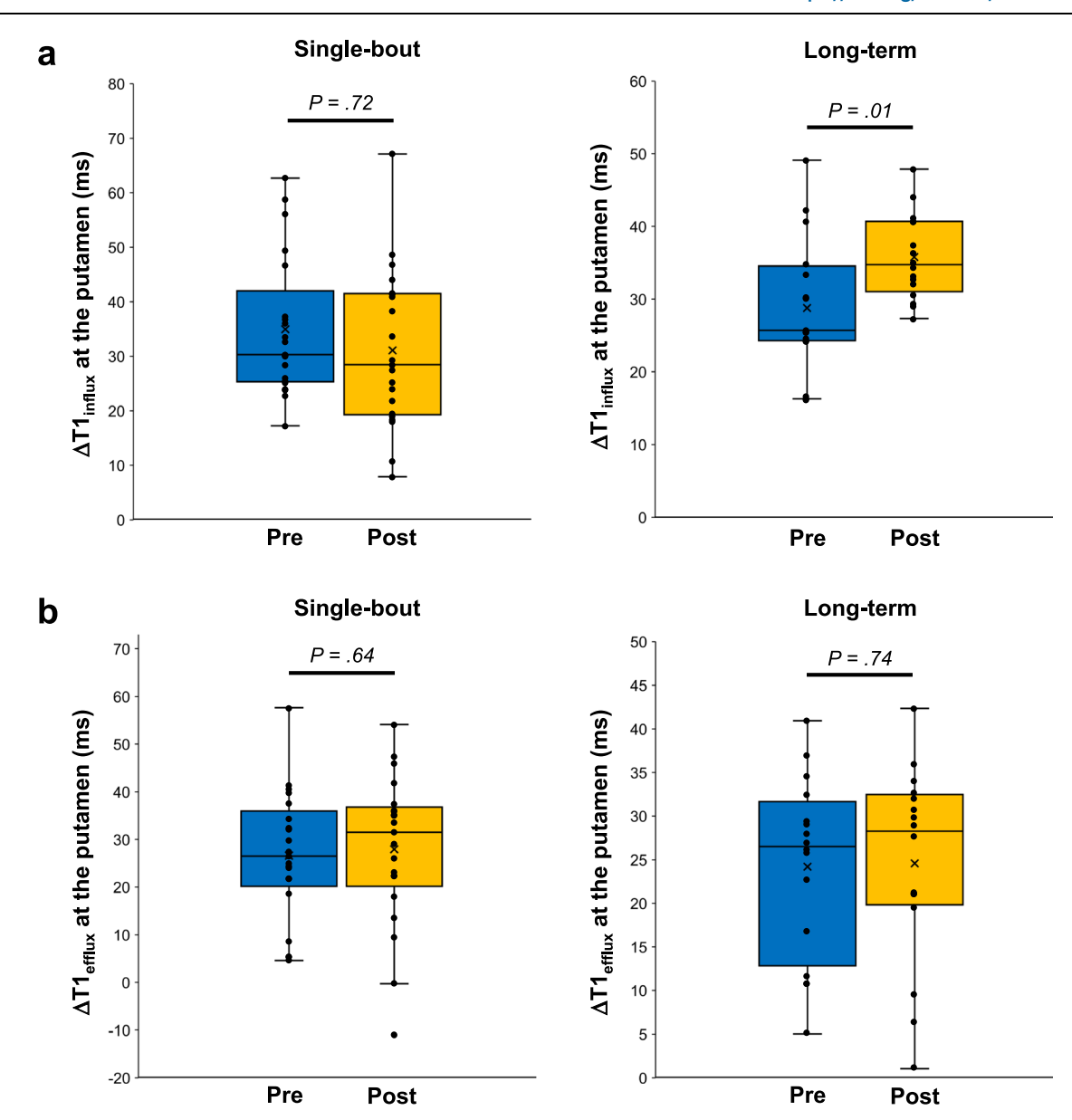


Fig. 1 | Changes in Δ T1 values (Δ T1_{influx} and Δ T1_{efflux}) at the putamen after exercise in each group (Single-bout [n = 21], long-term [n = 16]). Changes in Δ T1_{influx}(a) and Δ T1_{efflux}(b) values at the putamen after exercise are shown for each group. The line across the box denotes the median value, and the boundaries of the

box represent the 25th and 75th percentiles. The whiskers indicate the minimum and maximum values. The P values were calculated using the two-sided Wilcoxon signed-rank test. Source data are provided as a source data file.

exercise group. Among the 15 proteins whose expression changed only in the long-term exercise group, 5 proteins were up-regulated after exercise, whereas 10 proteins were down-regulated after exercise (Supplementary Table 3 and Supplementary Figs. 9 and 10).

Among the down-regulated long-term DEPs, S100A8 (ρ = -0.36, P = 0.03), S100A9 (ρ = -0.37, P = 0.03), DEFA1A3 (ρ = -0.32, P = 0.048), and PSMA3 (ρ = -0.35, P = 0.04) had significant negative correlations with Δ T1_{influx}. Among the up-regulated long-term DEPs, the J chain was positively correlated with the putative mLV PSC (ρ = 0.40, P = 0.02) (Fig. 5).

Discussion

In this study, we demonstrated the effects of physical exercise on both upstream and downstream brain waste clearance systems. Specifically, we sought to quantitatively assess the impact of physical exercise on putative glymphatic and mLV flow in healthy volunteers via noninvasive MR imaging techniques, such as intravenous contrast-enhanced dynamic T1 mapping, BB imaging, and interslice flow imaging. When

comparing two exercise protocols with varying durations and intensities, the clearance activities of both brain waste clearance systems were significantly enhanced in the 12-week long-term exercise group.

Most of the earlier studies on glymphatic flow acquired long-itudinal dynamic 3D T1-weighted imaging over a longer time period after intrathecal GBCA injection to examine the glymphatic influx and clearance (Supplementary Table 1). Instead of the dynamic T1-weighted imaging after intrathecal GBCA injection (off-label use of GBCA in most countries), we used an intravenous contrast-enhanced dynamic T1 mapping technique for quantitative evaluation of putative glymphatic activity and demonstrated the positive effect of long-term physical exercise on putative glymphatic influx, which is consistent with the results of other animal studies^{20–22}. One study reported that 6 weeks of voluntary wheel running exercise significantly attenuated the inflammatory activation of microglia and astrocytes in aged mice. The decrease in inflammatory activation improved astrocytic AQP4 expression and polarization, which in turn accelerated ISF drainage via the glymphatic system²⁰. Another study examined the effect of

Table 2 | Comparison of putative glymphatic flow between pre- and post-exercise states for each group

Parameter	Single-bout (n = 21) Pre-exercise	Long-term (n = 16) Post-exercise	P value ^a	Pre-exercise	Post-exercise	P valueª
Putamen						
ΔT1 _{influx}	30.3 (25.4–39.6)	28.4 (19.4-41.4)	0.72	25.7 (24.3-34.2)	34.7 (31.4–40.7)	0.01
ΔT1 _{efflux}	26.5 (20.1–35.1)	31.5 (21.2–36.4)	0.64	26.5 (12.8–31.7)	28.3 (19.8–32.5)	0.74
Cerebral GM						
ΔT1 _{influx}	66.9 (58.7–84.5)	71.7 (65.7–86.2)	0.17	61.4 (53.4–67.7)	60.8 (57.9–63.7)	1.00
ΔT1 _{efflux}	56.3 (46.2-75.1)	58.3 (51.6-64.0)	0.61	51.2 (43.7-57.7)	50.5 (47.7-55.2)	0.82

Data are reported as medians (IQRs).

^aThe P values were calculated using the two-sided Wilcoxon signed-rank test.

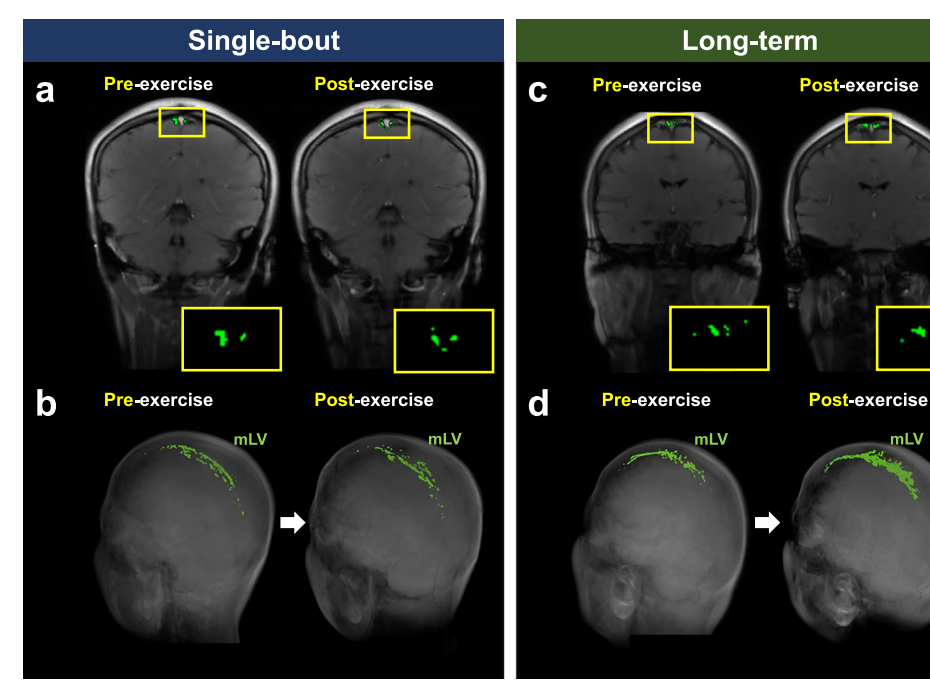


Fig. 2 | Changes in the mLV ROI size after exercise in representative participants in the single-bout and long-term exercise groups. 2D coronal IR-ALADDIN baseline images (**a**, **c**) and reconstructed 3D BB images (**b**, **d**) depict an increase in

the mLV ROI size after exercise in the long-term exercise group (\mathbf{c}, \mathbf{d}) but not in the single-bout exercise group (\mathbf{a}, \mathbf{b}) . mLV meningeal lymphatic vessels, ROI region-of-interest.

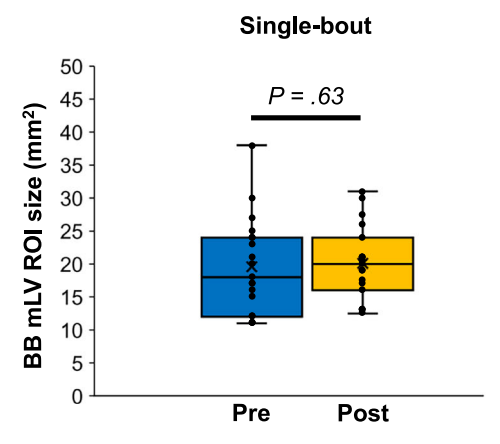
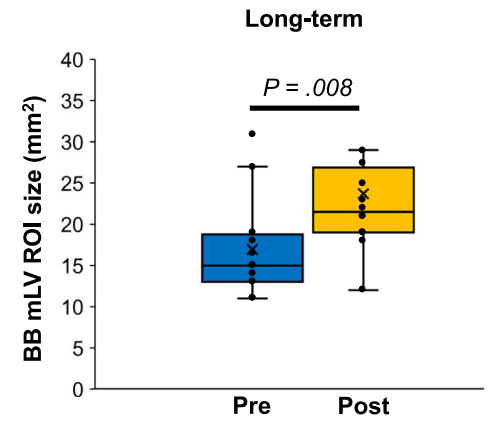


Fig. 3 | Changes in the mLV ROI size from BB imaging after exercise in each group (single-bout [n=19], long-term [n=12]). The line across the box denotes the median value, and the boundaries of the box represent the 25th and 75th percentiles. The whiskers indicate the minimum and maximum values. The P values



were calculated using the two-sided Wilcoxon signed-rank test. Source data are provided as a Source Data file. BB black-blood, mLV meningeal lymphatic vessels, ROI region-of-interest.

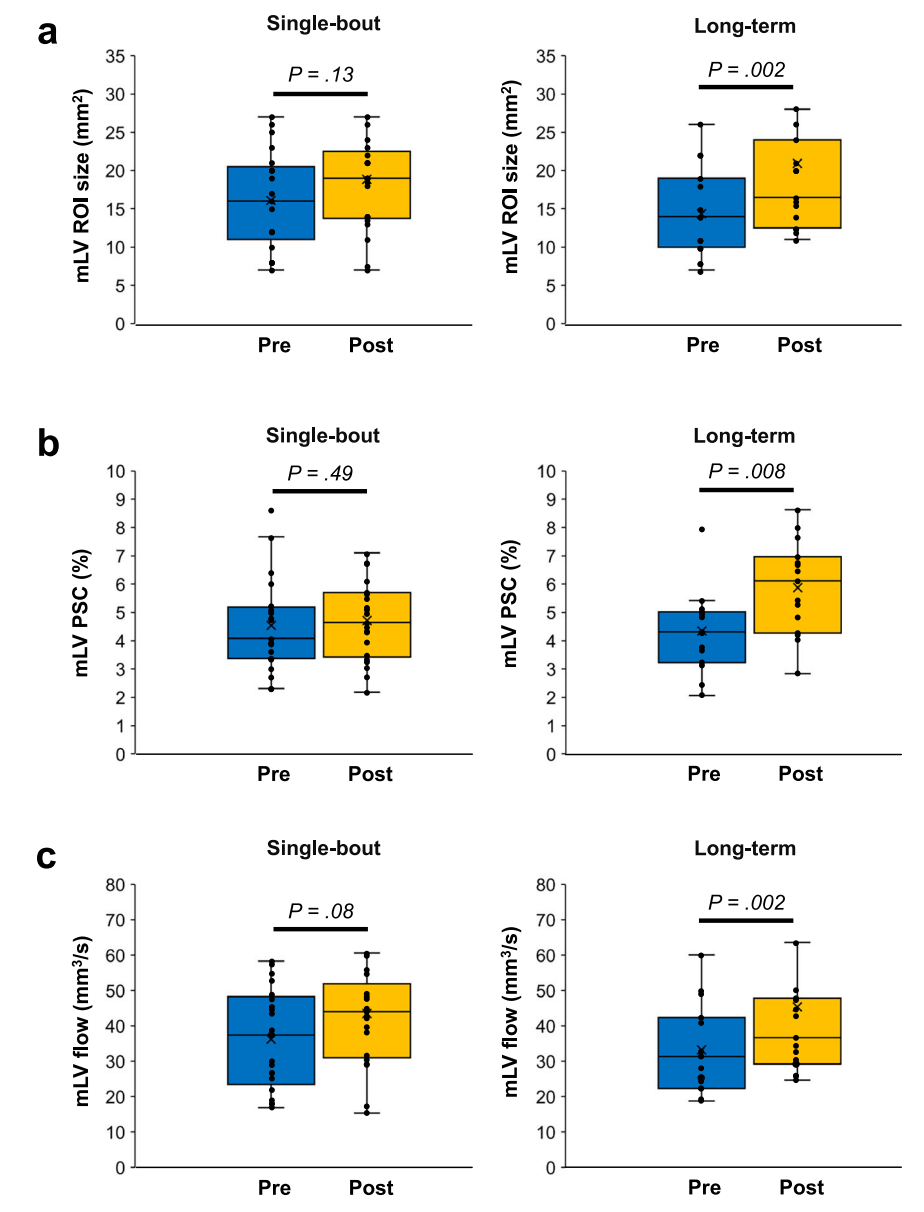


Fig. 4 | Changes in mLV imaging metrics (mLV ROI size, mLV PSC, and mLV flow) from IR-ALADDIN after exercise in each group (Single-bout [n=21], long-term [n=15]). Changes in the mLV ROI size (a), mLV PSC (b), and mLV flow (c) after exercise are shown for each group. The line across the box denotes the median value, and the boundaries of the box represent the 25th and 75th percentiles. The

whiskers indicate the minimum and maximum values. The P values were calculated using the two-sided Wilcoxon signed-rank test. Source data are provided as a Source Data file. mLV meningeal lymphatic vessels, PSC percent signal change, ROI region-of-interest.

voluntary running on glymphatic tracer influx in awake young mice to exclude confounding effects of aging and anesthesia²¹. The study reported a more than twofold increase in glymphatic influx in awake young mice after 5 weeks of voluntary wheel running, as compared with that in awake sedentary mice. Interestingly, contrary to findings in awake exercised mice, CSF tracer influx was reduced during active running. These results suggest that physiological adaptations to regular physical activity, such as cardiovascular changes, may enhance the glymphatic influx.

Human studies investigating the direct association between physical exercise and glymphatic flow are limited. However, Furby et al. reported that physical exercise increases cardiorespiratory fitness by increasing cerebral arterial compliance (i.e., lowering arterial wall stiffness)²³. In addition, it has been shown that arterial hypertension alters the form of the arterial traveling wave and causes arteries to expand and contract faster by increasing arterial stiffness in mice²⁴. The change in arterial waveform in turn reduced net CSF flow by

increasing CSF backflow. Given the relationship between arterial wall stiffness and net CSF flow, physical exercise may ultimately enhance glymphatic flow by increasing cerebral arterial compliance.

Based on the previous studies, the increased putative glymphatic influx at the putamen, as demonstrated by greater $\Delta T l_{\rm influx}$, may be attributed to two factors: (1) increased cerebral arterial compliance²³ and (2) augmented ISF drainage resulting from the attenuated inflammatory activation of microglia and astrocytes²⁴. The anti-inflammatory role of physical exercise is supported by the following results of our proteasome analysis: (1) S100A8, S100A9, DEFA1, DEFA3, and PSMA3 were down-regulated after long-term exercise and correlated with $\Delta T l_{\rm influx}$ at the putamen; (2) J chain was up-regulated after long-term exercise and correlated with putative mLV PSC. S100A8 and S100A9, cytoplasmic proteins abundant in neutrophils, are up-regulated during various inflammatory processes, stimulating leukocyte recruitment and cytokine secretion²⁵. DEFA1 and DEFA3 are primarily stored in azurophil granules of neutrophils and are released

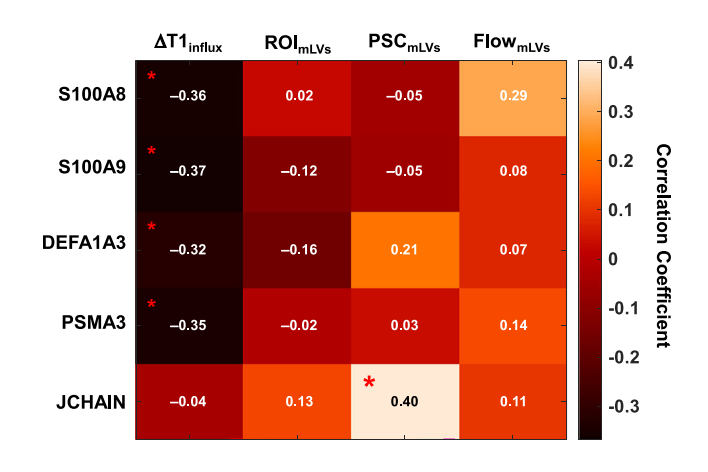


Fig. 5 | Heatmap displaying the correlation coefficients between differentially expressed proteins (DEPs) and MR imaging metrics of glymphatic and mLV flow. ROI_{mLVs} were calculated from BB imaging, whereas PSC_{mLVs} and Flow_{mLVs} were derived from IR-ALADDIN imaging. The P values were calculated using the two-sided Spearman's correlation test. Asterisks indicate statistical significance of P < 0.05. The raw data of mass spectrometry proteomics have been deposited to the ProteomeXchange Consortium via the PRIDE partner repository with the dataset identifier PXD058255. mLV meningeal lymphatic vessels, PSC percent signal change, ROI region-of-interest.

into circulation when neutrophils are activated by phagocytic stimuli such as infections²⁶. PSMA3 is a component of the proteasome complex that degrades proteins damaged by oxidative stress induced by inflammation²⁷. The J chain, a small polypeptide that regulates the polymer formation of immunoglobulins A and M, acts as a key protein in secretory immunity²⁸. Taken together, the up-regulation of the J chain in our study may reflect an enhancement of immunocompetence due to physical exercise²⁹. This enhancement could reduce the risk of inflammatory or infectious diseases, leading to a decrease in neutrophil activation and a reduction in the accumulation of damaged proteins (Supplementary Fig. 11).

For mLV imaging, Absinta et al., Park et al., Joo et al., and Jacob et al. compared 3D T1-weighted BB imaging before and after intravenous contrast enhancement to capture structural mLV images(Supplementary Table 1)^{15,17,18,30}. Ding et al. employed dynamic intravenous contrast-enhanced 3D BB imaging to observe rapid contrast enhancements in putative mLV areas. Meanwhile, Ringstad et al., Zhou et al., and Melin et al. applied dynamic intrathecal contrastenhanced 3D T1-weighted imaging and either or both of 3D BB and 3D FLAIR imaging to study CSF tracer efflux and parasagittal dural enhancements31-33. Combined acquisition of contrast-enhanced BB imaging and IR-ALADDIN MR imaging techniques provides a noninvasive means for obtaining structural and functional information on dorsal parasagittal putative mLVs. The observed increase in the ROI size of putative mLVs following long-term exercise, as shown in Figs. 3 and 4, may be a contributing factor to the enhanced putative mLV flow in our study. While the exact mechanisms remain unclear, one possible hypothesis is that long-term exercise might influence brain lymphangiogenesis, similar to findings in a previous study where swimming exercise enhanced VEGFR3 expression and promoted lymphangiogenesis in cardiac tissues³⁴ Moreover, Ding et al. reported that meningeal inflammation leads to the loss of tight junctions among meningeal lymphatic endothelial cells and, eventually, impaired mLV drainage in patients with idiopathic Parkinson's disease¹⁶. Given the accumulating evidence that physical exercise suppresses neuroinflammation³⁵, we speculate that long-term cycle ergometer exercise possibly decreased inflammation in the long-term exercise group. This reduction in inflammation could have led to increased

putative mLV flow, as indicated by the down-regulation of inflammation-related proteins in this study.

Decreased neuroinflammation through physical exercise has been shown to increase cognitive function in mice³⁵. While it has also been well documented that physical exercise, particularly aerobic exercise, lowers the risk of dementia and slows the progression of cognitive decline in patients with dementia^{36,37}, the key intermediate step between physical exercise and improved cognitive function in patients has not been well demonstrated. Our data provide evidence that increased putative glymphatic and mLV flow is likely the potential mechanism underlying the neuroprotective effects of exercise on cognition in humans. Therefore, our results highlight the importance of long-term, regular exercise interventions in the general population, as well as in patients with dementia.

Our study had several limitations. First, the study had a small sample size and included relatively healthy and young individuals. The inter-individual variability in exercise effects could affect the experimental result due to the small sample size. Furthermore, since glymphatic function and brain clearance mechanisms may vary with age, future studies that include larger sample sizes and participants across a broader age range are needed for the generalizability of this study. Second, we only investigated the effect of a single exercise modality (cycle ergometer) on the brain clearance systems. Third, even though participants were verbally instructed to abstain from consuming caffeine or alcohol, they were not closely monitored to ensure compliance. Therefore, the possibility remains that the changes observed could have been partly caused by the confounding factors.

Methods

Participants and approvals

This randomized clinical trial was approved by the institutional review board of Seoul National University Hospital (IRB No. 2011–064–1171), and written informed consent was obtained from all participants.

The participants were healthy volunteers aged 19-70 years, with the first participant enrolled on March 16, 2021, and the last participant enrolled on July 22, 2022. The inclusion criteria were as follows: (1) an age of 19-70 years, regardless of sex, and (2) no history of any kind of neurologic disease, sleep disorders, or other medical conditions. The exclusion criteria were as follows: (1) any contraindication to MR imaging, including a cardiac pacemaker implanted state or claustrophobia; (2) any contraindication to the use of the GBCA, such as renal failure or a past history of adverse reactions to the GBCA; (3) failure to complete the scheduled exercise sessions; (4) suboptimal MR image quality; and (5) incidentally detected brain lesions on MR imaging. Participants were enrolled regardless of sex, with sex determined by self-report. Gender was not explicitly considered or analyzed. While participant sex demographics were reported, no sex- or gender-based analyses were conducted due to the study's focus on exercise-induced brain clearance mechanisms. This approach aligns with ethical guidelines, and all individual-level data were anonymized.

Study design

The participants were randomly allocated into two groups, the single-bout and long-term exercise groups, at a 1:1 ratio. To minimize predictability in group assignment, a mixed block randomization method was employed with the block size set as 4 or 6, and the participants were allocated to the single-bout and long-term exercise groups at a 1:1 ratio within each block. Age (19–39 years vs 40–60 years vs 61 years and above) was considered a stratification factor. At baseline (pre-exercise state), physical fitness levels and the ability to engage in physical activity in adult populations were assessed with the IPAQ and PARQ (Physical Activity Readiness Questionnaire), and the participants' systolic and diastolic BP and HR were measured. Baseline glymphatic and mLV MR images were obtained with a 3 T imaging unit. Baseline venous blood sampling was performed for proteome analysis.

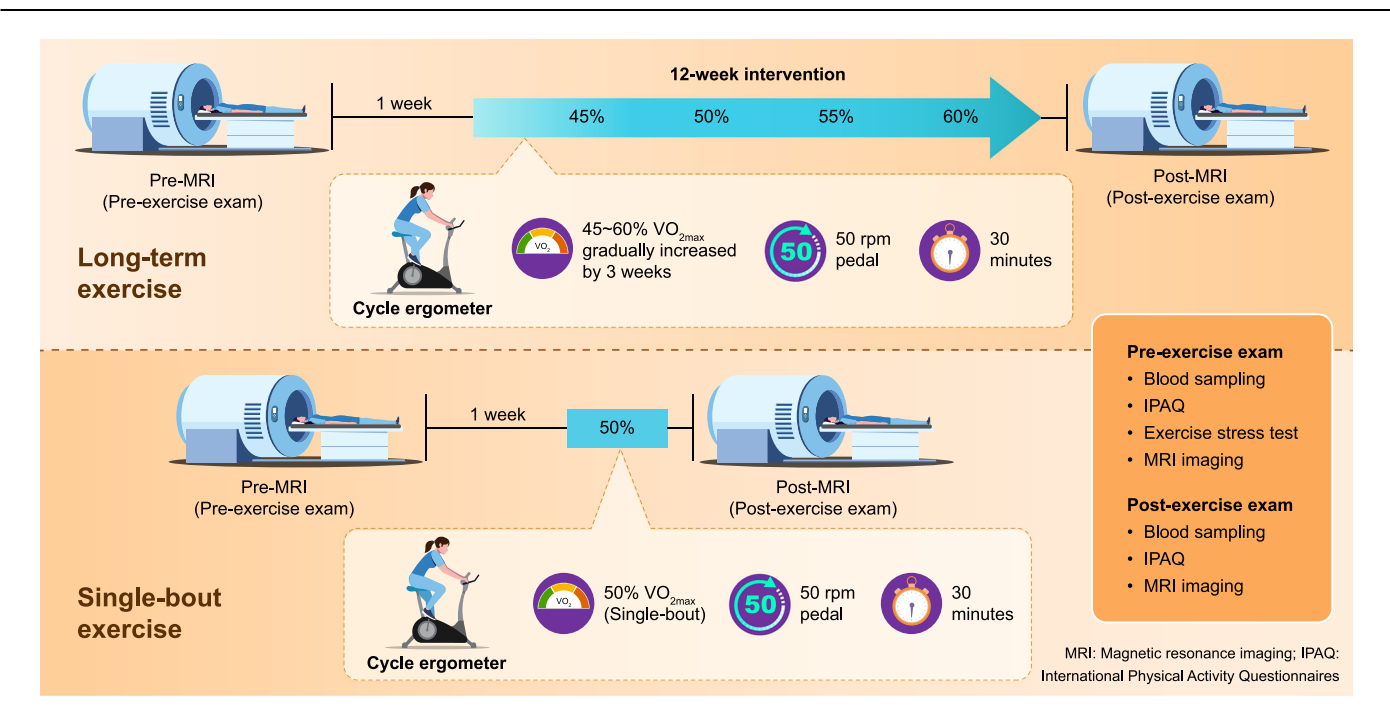


Fig. 6 | Illustration of the study design, including single-bout and long-term exercise schedules and pre- and post-exercise examinations. IPAQ international physical activity questionnaire.

To minimize the impact of inter-individual variability in exercise effects, we did not impose the same absolute exercise intensity on all participants. Instead, we assessed each participant's exercise capacity, heart rate (HR), and maximum oxygen consumption (VO_{2max}) to determine the appropriate exercise intensity for each participant. Subsequently, the single-bout exercise group participated in a single session of fixed-cycle ergometer (Monark Ergomedic 828E; Grimaldi Industri AB) exercise at an intensity corresponding to 50% of their VO_{2max}. This session occurred one week after the baseline MR imaging to consider the washout time for GBCAs. Meanwhile, the long-term exercise group participated in exercise sessions three times a week for a total of 12 weeks. Each session lasted for 30 min on the same cycle ergometer used by the single-bout exercise group. Initially, the exercise intensity was set at 45% of VO_{2max} and was progressively increased by 5% every three weeks, reaching 60% VO_{2max} during the final three weeks. HR and rate of perceived exertion were assessed at three time points: pre-exercise, during exercise (15 min after initiation), and postexercise (1 min after completion). After completing the exercise sessions, the IPAQ questionnaire, BP and HR measurements, venous blood sampling, and glymphatic and mLV MR imaging were repeated for all participants (Fig. 6). Additional details of the IPAQ questionnaire and exercise protocol are provided in the supplementary information.

MR imaging protocol

All MR imaging was performed with a 3 T imaging unit (TrioTim; Siemens Healthineers) using a 32-channel head coil. MRI scans were acquired before and after IV bolus injection of gadobutrol (Gadovist; Bayer Schering Pharma) at a dose of 0.1 mmol/kg of body weight. Precontrast MR imaging included three-dimensional (3D) T1-weighted fast spoiled gradient-echo (FSPGR), 3D BB T1-weighted fat-suppressed Cube motion-sensitization driven equilibrium (MSDE), IR-ALADDIN, and T1 mapping (magnetization prepared 2 rapid acquisition gradient echoes [MP2RAGE]) sequences. Postcontrast MR imaging included 3D BB T1-weighted fat-suppressed Cube MSDE sequence obtained after contrast injection, 3D T1-weighted FSPGR sequence, and T1 mapping obtained at 0.5 h and 12 h after contrast injection. The delayed scans were obtained after a normal night's sleep according to a previously established protocol¹⁴.

BB imaging acquisition

To serve as a structural reference for the putative mLV size obtained from IR-ALADDIN, we obtained the contrast-enhanced 3D BB T1-weighted fat-suppressed Cube MSDE 15 . The parameters for the 3D BB T1-weighted imaging were as follows: TR/TE = 620/15 ms, flip angle = variable, matrix size = 256 × 256, FOV = 250 × 250 mm², thickness = 1.2 mm, scan direction = sagittal, number of averages = 1, echo train length = 21, and total scan time = 5 min 35 s.

IR-ALADDIN technique

This study utilized the IR-ALADDIN technique for imaging parasagittal putative mLVs adjacent to the SSS¹⁹. This technique was developed for perfusion-weighted imaging to leverage the effects of inter-slice flow saturation, and the key feature of IR-ALADDIN is the use of preceding imaging slices as the labeling planes and long inversion time. The resulting proximity between the labeling and imaging slices along with the long inversion time make the technique highly sensitive to slow flow components, such as the mLV flow.

The IR-ALADDIN bSSFP imaging parameters were as follows: TR/ TE = 4.8/2.4 ms, flip angle = 60°, matrix size = 256 × 256, field of view (FOV) = 250 × 250 mm², thickness = 5 mm, gap = 5 mm (100% of the thickness), scan direction = coronal, phase encoding order = centric, slice-selective inversion time (TI) = 2300 ms, and PE direction = left–right. Each slice takes 3.5 s for acquisition. Asc/Dsc directional full sets (eight measurements) were acquired with nine image slices at a total scan time of 4 min and 29 s (Fig. 7a). To minimize variability in slice positioning, the IR-ALADDIN imaging slices were positioned consistently such that the middle slice (5th slice) passed through the center of the anterior commissure-posterior commissure line and covered the region of the pons (Fig. 7a).

MR imaging data analysis

Putative glymphatic and mLV MR images were analyzed by an experienced neuroradiologist (R.-E.Y. with 15 years of experience in neuroradiology) and an MR physicist (J.-H.K. with 6 years of experience in MR physics and engineering), who were blinded to the information regarding the group assignment and timing of MR imaging.

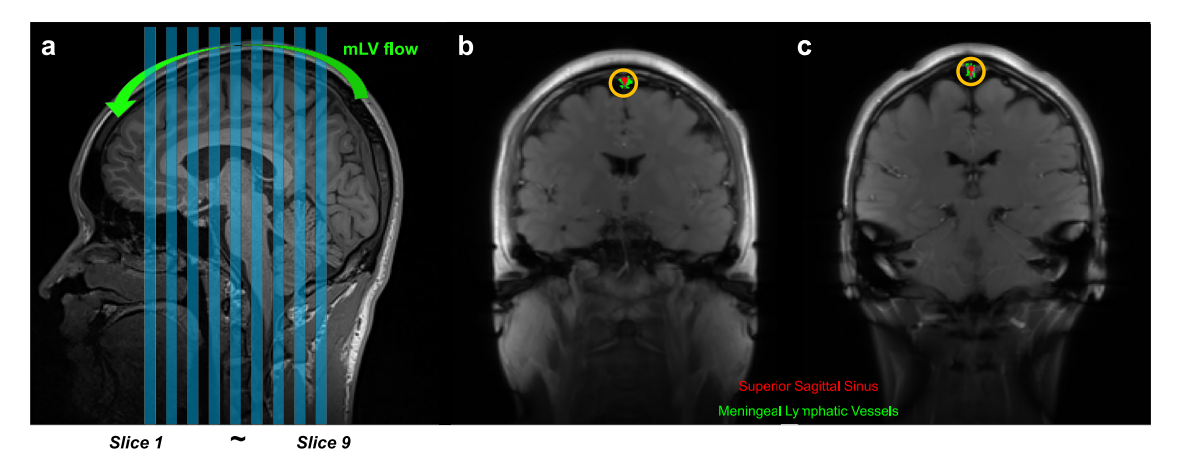


Fig. 7 | **Schematic image of IR-ALADDIN imaging protocol and ROIs of the dorsal parasagittal mLVs on IR-ALADDIN. a** The positions of nine coronal IR-ALADDIN images are shown as blue stripes. **b**, **c** IR-ALADDIN baseline images demonstrate the ROIs of the mLVs (green) and SSS (red). The ROIs of mLVs adjacent

to the SSS were segmented based on the distance from the SSS (yellow circle) and PSC on IR-ALADIDN. mLV meningeal lymphatic vessels, PSC percent signal change, ROI region-of-interest.

Putative glymphatic flow measurement using contrastenhanced dynamic T1 mapping

Automatic volumetric segmentation based on 3D T1-weighted images was performed using open-source software (FreeSurfer, version 6.0.0; Laboratory for Computational Neuroimaging). The two brain region masks (bilateral cerebral cortex and putamen) were selected as regions of interest (ROIs) based on the previous study and were co-registered with T1 maps using a commercial software package (NordicICE, version 4.1.2; NordicNeuroLab) to extract T1 values at the bilateral cerebral cortex and putamen¹⁴. The difference in section thickness between images was automatically corrected during coregistration.

The difference between the precontrast T1 value and the T1 value at 0.5 h after contrast injection (Δ T1_{influx}) was considered to reflect the initial influx of GBCA via the glymphatic pathway. Meanwhile, the difference between the T1 value at 0.5 h and the T1 value at 12 h after contrast injection (Δ T1_{efflux}) was viewed as an imaging finding indicative of the clearance of GBCA by the glymphatic pathway.

Putative mLV size measurement using BB imaging

Putative mLV structural images were obtained by subtracting the precontrast BB images from the postcontrast BB images. To minimize motion-related artifacts, intensity-based registration with rigid transformation was performed between the pre- and post-contrast images using a MATLAB-based approach. For postprocessing of the subtracted BB images, pixels within an inverted triangle-shaped ROI including the parasagittal dural space were sorted based on their signal intensity. Initially, pixels with intensities greater than 50% of the maximum intensity within the large ROI were included. Subsequently, the threshold ratio was manually adjusted only when necessary, based on the morphological appearance of the resulting ROI, to ensure that the segmented ROI reliably captured the putative mLV structures while minimizing the inclusion of non-relevant regions. After performing rigid registration between the 3D BB images and the 2D multislice IR-ALADDIN images, the putative mLV ROI size on the BB images was calculated at the target slice corresponding to the most similar location as compared with the IR-ALADDIN representative image. Due to the manual adjustments required during thresholding in BB imaging, two independent raters (R.-E.Y. with 15 years of experience in neuroradiology and J.-H.K. with 6 years of experience in MR physics and engineering) measured the putative BB ROI size on the center slices in the long-term exercise group. All image processing steps were performed using MATLAB R2023b (MathWorks).

Putative mLV flow measurement using IR-ALADDIN

For IR-ALADDIN data processing, four ascending (Asc) and four Dsc acquisitions were averaged separately and then subtracted from each other to maximize the flow signals that have directionality. To better visualize the mLVs, the images were displayed as PSC images (Asc –Dsc)/S×100, where Asc and Dsc represent the averaged ascending and Dsc images, respectively, and S represents the average of Asc and Dsc. The ROIs of putative mLVs adjacent to the SSS were semi-automatically segmented on the IR-ALADDIN. Initially, the ROI of the SSS region was identified based on the signal enhancement observed in the anterior to posterior PSC images of IR-ALADDIN. Subsequently, the putative mLV ROIs were defined as voxels with PSC values ranging from 1% to 9% at a distance of less than 3–5 mm from the segmented SSS ROI (Fig. 7b, c)¹⁹.

The PSC values of putative mLVs measured by IR-ALADDIN were converted to flow velocities based on the correspondence graph between the PSC and flow velocity reported in a previous study¹⁹. The cross-sectional flow of dorsal parasagittal putative mLVs was calculated by multiplying the putative mLV ROIs by the flow velocity measured on IR-ALADDIN.

Since the center slices of IR-ALADDIN were positioned based on the anatomical criteria (Fig. 7a), we used one representative slice of the center slices (4th–6th) as the target slice for mLV processing in IR-ALADDIN to minimize the measurement variability. The results obtained using the representative slice were similar to those from the full set of center slices (Supplementary Figs. 7, 8, and Supplementary Table 4). All image processing steps were performed using MATLAB R2023b (MathWorks).

Proteome analysis

Blood samples were collected before and after exercise from both the single-bout and long-term exercise groups. For each participant, 9 cc of blood was drawn from the antecubital vein and subjected to a 10-min centrifugation at 845 g to separate the serum into 2 mL of SST and 1 mL of NaF. Before protein sample analysis, we preserved the samples at 4 °C and the frozen samples at -70 °C. Proteome analysis was performed using data-independent acquisition. Details of the proteome analysis are provided in the supplementary information.

Statistical analysis

The statistical software MedCalc (version 19.2.0; MedCalc Software) and MATLAB R2023b (Mathworks) were used for all statistical analyses. A post hoc power calculation indicated that a sample size of 16 (long-term exercise participants) had approximately 100% power to detect an effect size of 3.5 in regional $\Delta T1_{influx}$ using two-sided Wilcoxon signed rank test with a significance level of .05 based on the effect size, which was calculated by using the mean and SD estimated from the sample size of $\Delta T1_{influx}$ values in a previous study¹⁴. After assessing the data normality with the Kolmogorov-Smirnov test, non-parametric data were reported as the median and IQR, while parametric data were presented as the mean ± standard deviation. Clinical data, including age, sex, height, weight, and VO_{2 max} were compared between the single-bout and longterm exercise groups using the two-sided Fisher exact test for categorical variables and the two-sided Mann-Whitney U test for continuous variables. For each group, systolic and diastolic BPs, HR, and imaging metrics for putative glymphatic and mLV flow were compared between pre- and post-exercise states using the two-sided Wilcoxon signed-rank test. Protein expression data were compared between pre- and postexercise states for each group using a two-sided t-test. The criterion for DEPs was set as an adjusted P value (false discovery rate) less than .05. The change in DEP intensity after exercise was correlated with the change in MR imaging metrics using two-sided Spearman's correlation. A two-sided intraclass correlation coefficient was calculated to determine the interrater agreement for manual adjustments required during thresholding in BB imaging. P values less than .05 were considered to be statistically significant in all tests.

Reporting summary

Further information on research design is available in the Nature Portfolio Reporting Summary linked to this article.

Data availability

The mass spectrometry proteomics data have been deposited to the ProteomeXchange Consortium via the PRIDE partner repository with the dataset identifier PXD058255. The individual subject data are available under restricted access due to privacy and institutional review board requirements, and access can be obtained by contacting the corresponding authors. Requests should include a brief description of the proposed research and evidence of institutional review board (IRB) or ethics committee approval from the requesting institution. Source data are provided with this paper. The processed MRI data are provided in the Supplementary Information and Source Data file. Source data are provided with this paper.

References

- Iliff, J. J. et al. A paravascular pathway facilitates CSF flow through the brain parenchyma and the clearance of interstitial solutes, including amyloid β. Sci. Transl. Med. 4, 147ra111 (2012).
- Louveau, A. et al. Structural and functional features of central nervous system lymphatic vessels. *Nature* 523, 337–341 (2015).
- Aspelund, A. et al. A dural lymphatic vascular system that drains brain interstitial fluid and macromolecules. J. Exp. Med. 212, 991–999 (2015).
- Jessen, N. A., Munk, A. S. F., Lundgaard, I. & Nedergaard, M. The glymphatic system: a beginner's guide. *Neurochem. Res.* 40, 2583–2599 (2015).
- Hershenhouse, K. S., Shauly, O., Gould, D. J. & Patel, K. M. Meningeal lymphatics: a review and future directions from a clinical perspective. *Neurosci. Insights* 14, 1179069519889027 (2019).
- Ahn, J. H. et al. Meningeal lymphatic vessels at the skull base drain cerebrospinal fluid. *Nature* 572, 62–66 (2019).
- Hu, X. et al. Meningeal lymphatic vessels regulate brain tumor drainage and immunity. Cell Res. 30, 229–243 (2020).

- Tavares, G. A. & Louveau, A. Meningeal lymphatics: an immune gateway for the central nervous system. Cells 10, 3385 (2021).
- das Neves, S. P., Delivanoglou, N. & Da Mesquita, S. CNS-draining meningeal lymphatic vasculature: roles, conundrums and future challenges. Front Pharm. 12, 655052 (2021).
- Tian, Y., Zhao, M., Chen, Y., Yang, M. & Wang, Y. The Underlying role of the glymphatic system and meningeal lymphatic vessels in cerebral small vessel disease. *Biomolecules* 12, 748 (2022).
- Silva, I., Silva, J., Ferreira, R. & Trigo, D. Glymphatic system, AQP4, and their implications in Alzheimer's disease. *Neurol. Res. Pract.* 3, 1–9 (2021).
- Agarwal, N. et al. Current understanding of the anatomy, physiology, and magnetic resonance imaging of neurofluids: update from the 2022 "ISMRM Imaging Neurofluids Study group" workshop in Rome. J. Magn. Reson. Imaging 59, 431–449 (2024).
- Da Mesquita, S., Fu, Z. & Kipnis, J. The meningeal lymphatic system: a new player in neurophysiology. Neuron 100, 375–388 (2018).
- Lee, S. et al. Contrast-enhanced MRI T1 mapping for quantitative evaluation of putative dynamic glymphatic activity in the human brain in sleep-wake states. *Radiology* 300, 661–668 (2021).
- Absinta, M. et al. Human and nonhuman primate meninges harbor lymphatic vessels that can be visualized noninvasively by MRI. *Elife* 6, e29738 (2017).
- Ding, X.-B. et al. Impaired meningeal lymphatic drainage in patients with idiopathic Parkinson's disease. Nat. Med. 27, 411–418 (2021).
- 17. Jacob, L. et al. Conserved meningeal lymphatic drainage circuits in mice and humans. *J. Exp. Med.* **219**, e20220035 (2022).
- Park, M., Kim, J. W., Ahn, S. J., Cha, Y. J. & Suh, S. H. Aging is positively associated with peri-sinus lymphatic space volume: assessment using 3T black-blood MRI. J. Clin Med. 9, 3353 (2020).
- Kim, J.-H., Yoo, R.-E., Choi, S. H. & Park, S.-H. Non-invasive flow mapping of parasagittal meningeal lymphatics using 2D interslice flow saturation MRI. Fluids Barriers CNS 20, 37 (2023).
- He, X.-f. et al. Voluntary exercise promotes glymphatic clearance of amyloid beta and reduces the activation of astrocytes and microglia in aged mice. Front. Mol. Neurosci. 10, 144 (2017).
- von Holstein-Rathlou, S., Petersen, N. C. & Nedergaard, M. Voluntary running enhances glymphatic influx in awake behaving, young mice. Neurosci. Lett. 662, 253–258 (2018).
- 22. Li, M. et al. Voluntary wheel exercise improves glymphatic clearance and ameliorates colitis-associated cognitive impairment in aged mice by inhibiting TRPV4-induced astrocytic calcium activity. Exp. Neurol. **376**, 114770 (2024).
- Furby, H. V., Warnert, E. A., Marley, C. J., Bailey, D. M. & Wise, R. G. Cardiorespiratory fitness is associated with increased middle cerebral arterial compliance and decreased cerebral blood flow in young healthy adults: a pulsed ASL MRI study. *J. Cereb. Blood Flow. Metab.* 40, 1879–1889 (2020).
- Mestre, H. et al. Flow of cerebrospinal fluid is driven by arterial pulsations and is reduced in hypertension. *Nat. Commun.* 9, 4878 (2018).
- 25. Wang, S. et al. S100A8/A9 in Inflammation. *Front. Immunol.* **9**, 1298 (2018).
- 26. Ganz, T. Defensins: antimicrobial peptides of innate immunity. *Nat. Rev. Immunol.* **3**, 710–720 (2003).
- Zhang, J. et al. Proteasome-associated syndromes: updates on genetics, clinical manifestations, pathogenesis, and treatment. J. Clin. Immunol. 44, 88 (2024).
- 28. Johansen, F. E., Braathen, R. & Brandtzaeg, P. Role of J chain in secretory immunoglobulin formation. *Scand. J. Immunol.* **52**, 240–248 (2000).
- Scheffer, D. D. L. & Latini, A. Exercise-induced immune system response: anti-inflammatory status on peripheral and central organs. *Biochim. Biophys. Acta Mol. Basis Dis.* 1866, 165823 (2020).

- Joo, B., Park, M., Ahn, S. J. & Suh, S. H. Assessment of meningeal lymphatics in the parasagittal dural space: a prospective feasibility study using dynamic contrast-enhanced magnetic resonance imaging. *Korean J. Radiol.* 24, 444 (2023).
- 31. Ringstad, G. & Eide, P. K. Cerebrospinal fluid tracer efflux to parasagittal dura in humans. *Nat. Commun.* **11**, 354 (2020).
- 32. Zhou, Y. et al. Impairment of the glymphatic pathway and putative meningeal lymphatic vessels in the aging human. *Ann. Neurol.* **87**, 357–369 (2020).
- Melin, E., Eide, P. K. & Ringstad, G. In vivo assessment of cerebrospinal fluid efflux to nasal mucosa in humans. Sci. Rep. 10, 14974 (2020).
- Bei, Y. et al. Lymphangiogenesis contributes to exercise-induced physiological cardiac growth. J. Sport Health Sci. 11, 466–478 (2022).
- 35. Wang, M., Zhang, H., Liang, J., Huang, J. & Chen, N. Exercise suppresses neuroinflammation for alleviating Alzheimer's disease. *J. Neuroinflammation* **20**, 76 (2023).
- Ahlskog, J. E., Geda, Y. E., Graff-Radford, N. R. & Petersen, R. C. Physical exercise as a preventive or disease-modifying treatment of dementia and brain aging. *Mayo Clin. Proc.* 86, 876–884 (2011).
- Meng, Q., Lin, M.-S. & Tzeng, I.-S. Relationship between exercise and Alzheimer's disease: a narrative literature review. Front. Neurosci. 14, 131 (2020).

Acknowledgements

The authors express their sincere gratitude to all participants involved in the study. Special thanks are to Yunhee Choi from the Division of Medical Statistics, Medical Research Collaborating Center, Seoul National University Hospital, for conducting the sample size and power analysis of our dataset, which greatly contributed to this work. This study was supported by Basic Science Research Program through the National Research Foundation of Korea (NRF) funded by the Ministry of Science, ICT & Future Planning (NRF-2020R1A2C2008949: S.H.C, RS-2023-00242754: S.H.C. RS-2023-00224382; S.H.C. RS-2023-00207783; S.-H.P. S.H.C. NRF-2022R1I1A4053049: H.Y.M, 2022R1A5A8019303: H.Y.M, NRF-2023R1A2C3003250: R.-E.Y, RS-2024-00358082: J.-H.K), by Korea Basic Science Institute (National research Facilities and Equipment Center) grant funded by the Ministry of Education (RS-2024-00435727: S.H.C), by Samsung Research Funding & Incubation Center of Samsung Electronics under Project Number SRFC-IT2201-04: S.H.C, by Seoul National University Hospital (SNUH) GE center grant (1820230040: S.H.C), by the Institute for Basic Science (IBS-R006-D1: S.H.C), by Seoul National University Research Grant (800-20210534: S.H.C), and by grant no. 0320230270 from the SNUH Research Fund (R.-E.Y).

Author contributions

R.-E.Y., J.-H.K., and H.Y.M. contributed equally to this work. R.-E.Y., J.-H.K., H.Y.M., Y.K., S.-H.P. and S.H.C. designed the study. R.-E.Y., J.Y.P., H.Y.M.,

Y.K., and S.H.C. recruited study subjects and prepared the MRI data. R.-E.Y., J.-H.K., J.Y.P., H.Y.M., Y.K., S.-H.P., and S.H.C. performed data generation, curation, and analysis. S.C., H.-S.S., and D.H. performed proteomics data generation, curation, and analysis. R.-E.Y., J.-H.K., and J.Y.P. wrote the manuscript. All authors reviewed, edited, and approved the manuscript. R.-E.Y., H.Y.M., Y.K., S.-H.P., and S.H.C. provided supervision and funding support.

Competing interests

The authors declare no competing interests.

Additional information

Supplementary information The online version contains supplementary material available at https://doi.org/10.1038/s41467-025-58726-1.

Correspondence and requests for materials should be addressed to Yukyoum Kim, Sung-Hong Park or Seung Hong Choi.

Peer review information *Nature Communications* thanks Koichi Oshio and the other, anonymous, reviewer(s) for their contribution to the peer review of this work. A peer review file is available.

Reprints and permissions information is available at http://www.nature.com/reprints

Publisher's note Springer Nature remains neutral with regard to jurisdictional claims in published maps and institutional affiliations.

Open Access This article is licensed under a Creative Commons Attribution-NonCommercial-NoDerivatives 4.0 International License, which permits any non-commercial use, sharing, distribution and reproduction in any medium or format, as long as you give appropriate credit to the original author(s) and the source, provide a link to the Creative Commons licence, and indicate if you modified the licensed material. You do not have permission under this licence to share adapted material derived from this article or parts of it. The images or other third party material in this article are included in the article's Creative Commons licence, unless indicated otherwise in a credit line to the material. If material is not included in the article's Creative Commons licence and your intended use is not permitted by statutory regulation or exceeds the permitted use, you will need to obtain permission directly from the copyright holder. To view a copy of this licence, visit https://creativecommons.org/licenses/by-nc-nd/4.0/.

© The Author(s) 2025